Spectroscopy of ytterbium-doped tantalum pentoxide rib waveguides on silicon

A. Aghajani,[1*] G. S. Murugan,[1] N. P. Sessions,[1] S. J. Pearce,[3] V. Apostolopoulos[2] and J. S. Wilkinson[1]

[1]*Optoelectronics Research Centre, University of Southampton, Southampton, SO17 1BJ, UK*
[2]*School of Physics and Astronomy, University of Southampton, Southampton, SO17 1BJ, UK*
[3]*Electronics and Computer Science, University of Southampton, Southampton, SO17 1BJ, UK*
[*]*aa15v07@soton.ac.uk*

Abstract: The design, fabrication and spectroscopic characterization of ytterbium-doped Ta_2O_5 rib waveguide are described. The waveguides are fabricated on silicon substrates and operate in a single mode at wavelengths above 970 nm. The peak absorption cross-section was measured to be 2.75 $\times 10^{-20}$ cm^2 at 975 nm. The emission spectrum was found to have a broad fluorescence spanning from 990 nm to 1090 nm with the fluorescence emission peak occurring at a wavelength of 976 nm. The excited-state life time was measured to be approximately 260 µs.

OCIS codes: (130.0130) Integrated optics; (160.3130) Integrated optics materials; (230.7380) Waveguides, channeled; (300.6360) Spectroscopy, laser; (140.3615) Lasers, ytterbium.

References and links

1. S. Ohara and Y. Kuroiwa, "Highly ytterbium-doped bismuth-oxide-based fiber," Opt. Express **17**(16), 14104–14108 (2009).
2. N. V. Kuleshov, A. A. Lagatsky, A. V. Podlipensky, V. P. Mikhailov, and G. Huber, "Pulsed laser operation of Y b-dope d $KY(WO_4)_2$ and $KGd(WO_4)_2$," Opt. Lett. **22**(17), 1317–1319 (1997).
3. D. Geskus, S. Aravazhi, S. M. García-Blanco, and M. Pollnau, "Giant optical gain in a rare-earth-ion-doped microstructure," Adv. Mater. **24**(10), OP19–OP22 (2012).
4. J. I. Mackenzie, "Dielectric solid-state planar waveguide lasers: a review," IEEE J. Sel. Top. Quantum Electron. **13**(3), 626–637 (2007).
5. D. C. Hanna, J. K. Jones, A. C. Large, D. P. Shepherd, A. C. Tropper, P. J. Chandler, M. J. Rodman, P. D. Townsend, and L. Zhang, "Quasi 3-level 1.03µm laser operation of a planar ion-implanted Yb-YAG waveguide," Opt. Commun. **99**(3–4), 211–215 (1993).
6. J. Siebenmorgen, T. Calmano, K. Petermann, and G. Huber, "Highly efficient Yb:YAG channel waveguide laser written with a femtosecond-laser," Opt. Express **18**(15), 16035–16041 (2010).
7. J. K. Jones, J. P. de Sandro, M. Hempstead, D. P. Shepherd, A. C. Large, A. C. Tropper, and J. S. Wilkinson, "Channel waveguide laser at 1 µm in Yb-indiffused $LiNbO_3$," Opt. Lett. **20**(13), 1477–1479 (1995).
8. M. Fujimura, H. Tsuchimoto, and T. Suhara, "Yb-diffused $LiNbO_3$ annealed/proton-exchanged waveguide lasers," IEEE Photon. Technol. Lett. **17**(1), 130–132 (2005).
9. D. Geskus, S. Aravazhi, E. Bernhardi, C. Grivas, S. Harkema, K. Hametner, D. Gunther, K. Wörhoff, and M. Pollnau, "Low-threshold, highly efficient Gd^{3+}, Lu^{3+} co-doped $KY(WO_4)_2$:Yb^{3+} planar waveguide lasers," Laser Phys. Lett. **6**(11), 800–805 (2009).
10. F. M. Bain, A. A. Lagatsky, R. R. Thomson, N. D. Psaila, N. V. Kuleshov, A. K. Kar, W. Sibbett, and C. T. A. Brown, "Ultrafast laser inscribed Yb:$KGd(WO_4)_2$ and Yb:$KY(WO_4)_2$ channel waveguide lasers," Opt. Express **17**(25), 22417–22422 (2009).
11. A. Choudhary, W. Bolaños, P. Kannan, J. J. Carvajal, M. Aguilo, F. Diaz, and D. P. Shepherd, "Low-threshold, mirrorless emission at 981 nm in an Yb, Gd, Lu:KYW inverted rib waveguide laser," Conference on Solid State Lasers XXII - Technology and Devices, San Francisco, USA (2013).
12. W. Bolaños, F. Starecki, A. Braud, J.-L. Doualan, R. Moncorgé, and P. Camy, "2.8 W end-pumped Yb^{3+}:$LiYF_4$ waveguide laser," Opt. Lett. **38**(24), 5377–5380 (2013).
13. C. Florea and K. A. Winick, "Ytterbium-doped glass waveguide laser fabricated by ion-exchange," J. Lightwave Technol. **17**(9), 1593–1601 (1999).
14. M. Ams, P. Dekker, G. D. Marshall, and M. J. Withford, "Monolithic 100 mW Yb waveguide laser fabricated using the femtosecond-laser direct-write technique," Opt. Lett. **34**(3), 247–249 (2009).

#212073 - $15.00 USD Received 15 May 2014; revised 20 Jun 2014; accepted 20 Jun 2014; published 3 Jul 2014

15. A. A. Lagatsky, A. Choudhary, P. Kannan, D. P. Shepherd, W. Sibbett, and C. T. A. Brown, "Fundamentally mode-locked, femtosecond waveguide oscillators with multi-gigahertz repetition frequencies up to 15 GHz," Opt. Express **21**(17), 19608–19614 (2013).
16. R. Mary, S. J. Beecher, G. Brown, R. R. Thomson, D. Jaque, S. Ohara, and A. K. Kar, "Compact, highly efficient ytterbium doped bismuthate glass waveguide laser," Opt. Lett. **37**(10), 1691–1693 (2012).
17. E. H. Bernhardi, H. A. G. M. van Wolferen, K. Wörhoff, R. M. de Ridder, and M. Pollnau, "Highly efficient, low-threshold monolithic distributed-Bragg-reflector channel waveguide laser in Al_2O_3:Yb^{3+}," Opt. Lett. **36**(5), 603–605 (2011).
18. J. S. Levy, A. Gondarenko, M. A. Foster, A. C. Turner-Foster, A. L. Gaeta, and M. Lipson, "CMOS-compatible multiple-wavelength oscillator for on-chip optical interconnects," Nat. Photonics **4**(1), 37–40 (2010).
19. G. N. van den Hoven, R. J. I. M. Koper, A. Polman, C. van Dam, J. M. W. van Uffelen, and M. K. Smit, "Net optical gain at 1.53 μm in Er-doped Al_2O_3 waveguides on silicon," Appl. Phys. Lett. **68**(14), 1886–1888 (1996).
20. C. Y. Tai, J. S. Wilkinson, N. M. B. Perney, M. C. Netti, F. Cattaneo, C. E. Finlayson, and J. J. Baumberg, "Determination of nonlinear refractive index in a Ta_2O_5 rib waveguide using self-phase modulation," Opt. Express **12**(21), 5110–5116 (2004).
21. J. D. B. Bradley, R. Stoffer, L. Agazzi, F. Ay, K. Wörhoff, and M. Pollnau, "Integrated Al_2O_3:Er^{3+} ring lasers on silicon with wide wavelength selectivity," Opt. Lett. **35**(1), 73–75 (2010).
22. B. Unal, M. C. Netti, M. A. Hassan, P. J. Ayliffe, M. D. B. Charlton, F. Lahoz, N. M. B. Perney, D. P. Shepherd, C.-Y. Tai, J. S. Wilkinson, and G. J. Parker, "Neodymium-doped tantalum pentoxide waveguide lasers," J. Quantum Electron. **41**(12), 1565–1573 (2005).
23. A. Z. Subramanian, C. J. Oton, D. P. Shepherd, and J. S. Wilkinson, "Erbium-doped waveguide laser in tantalum pentoxide," Photon. Technol. Lett. **22**(21), 1571–1573 (2010).
24. C. Chaneliere, J. L. Autran, R. A. B. Devine, and B. Balland, "Tantalum pentoxide (Ta_2O_5) thin films for advanced dielectric applications," Mater. Sci. Eng. Rep. **22**(6), 269–322 (1998).
25. A. Subramanian, "Tantalum pentoxide waveguide amplifier and laser for planar lightwave circuits," Ph.D. thesis, University of Southampton, UK (2011).
26. D. N. Christodoulides, I. C. Khoo, G. J. Salamo, G. I. Stegeman, and E. W. Van Stryland, "Nonlinear refraction and absorption: mechanisms and magnitudes," Adv. Opt. Photon. **2**(1), 60–200 (2010).
27. R. Soref, J. Schmidtchen, and K. Petermann, "Large single-mode rib waveguides in GeSi-Si and Si-on-SiO_2," J. Quantum Electron. **27**(8), 1971–1974 (1991).
28. A. Z. Subramanian, G. S. Murugan, M. N. Zervas, and J. S. Wilkinson, "Spectroscopy, modeling and performance of erbium-doped Ta_2O_5 waveguide amplifiers," J. Lightwave Technol. **30**(10), 1455–1462 (2012).
29. D. E. McCumber, "Einstein relations connecting broadband emission and absorption spectra," Phys. Rev. **136**(4A), A954–A957 (1964).
30. Y. Yu, Y. Huang, L. Zhang, Z. Lin, and G. Wang, "Growth and spectral assessment of Yb^{3+}-doped $KBaGd(MoO_4)_3$ crystal: a candidate for ultrashort pulse and tunable lasers," PLoS ONE **8**(1), e54450 (2013).
31. R. Paschotta, J. Nilsson, A. C. Tropper, and D. C. Hanna, "Ytterbium-doped fiber amplifiers," IEEE J. Quantum Electron. **33**(7), 1049–1056 (1997).
32. C. Hönninger, R. Paschotta, M. Graf, F. Morier-Genoud, G. Zhang, M. Moser, S. Biswal, J. Nees, A. Braun, G. A. Mourou, I. Johannsen, A. Giesen, W. Seeber, and U. Keller, "Ultrafast ytterbium-doped bulk lasers and laser amplifiers," Appl. Phys. B **69**(1), 3–17 (1999).
33. J. Y. Allain, M. Monerie, and H. Poignant, "Ytterbium-doped fluoride fibre laser operating at 1.02 μm," Electron. Lett. **28**(11), 988–989 (1992).
34. P. Nandi and G. Jose, "Ytterbium-Doped P_2O_5 -TeO_5 Glass for Laser Applications," IEEE J. Quantum Electron. **42**(11), 1115–1121 (2006).
35. N. V. Kuleshov, A. A. Lagatsky, A. V. Podlipensky, V. P. Mikhailov, and G. Huber, "Pulsed laser operation of Y b-dope d $KY(WO_4)_2$ and $KGd(WO_4)_2$," Opt. Lett. **22**(17), 1317–1319 (1997).
36. W. F. Krupke, "Ytterbium solid-state lasers. the first decade," IEEE J. Sel. Top. Quantum Electron. **6**(6), 1287–1296 (2000).
37. T. Y. Fan, "Quasi-three-level lasers" in *Solid State Lasers: New Development and Applications*, M. Inguscio and R. Wallenstein, eds. (Plenum Press, 1993)

1. Introduction

Yb-doped optical materials have found widespread application for lasers emitting at wavelengths near 1 μm in bulk, disk and fiber configurations. Their attractive properties include broad absorption near 0.98 μm for optical pumping from low-cost semiconductor sources, long excited-state lifetime for energy storage, broadband gain for wide wavelength selection, tunability and modelocking, a low quantum defect for good power-handling ability and lack of excited-state absorption or significant concentration-quenching effects, for efficient operation. Large absorption and emission cross-sections in several materials such as bismuthate glasses [1] and double tungstate crystals [2], lead to compact devices with the potential for very high gain coefficients. Gain coefficients close to 1000 dB/cm have been

#212073 - $15.00 USD Received 15 May 2014; revised 20 Jun 2014; accepted 20 Jun 2014; published 3 Jul 2014

measured for the latter, comparable with semiconductor devices [3]. Efficient, low threshold, operation of this quasi-three-level laser system is enhanced by incorporation in a waveguide configuration, due to the excellent pump/signal mode overlap and tight, diffraction-free, containment of the modes yielding high inversion at low pump powers. While planar waveguides have the disadvantage of higher loss coefficients when compared with optical fibers, this is of minor importance in the case of a high-gain system such as Yb^{3+} (in contrast to Er^{3+}) and the planar configuration has the further advantages of monolithic integration of mass-produced devices and of straightforward heat removal [4]. Many host materials have been exploited in the realisation of Yb-doped waveguide lasers and amplifiers, including YAG [5,6], $LiNbO_3$ [7,8], $KGd(WO_4)_2$ [9–11], $LiYF_4$ [12], silicate [13], phosphate [14,15] and bismuthate glasses [16] and Al_2O_3 [17]. Waveguide materials and processes that are compatible with silicon processing are strongly favoured for low-cost mass-manufacture. Silicon waveguides themselves are unsuitable for handling wavelengths below 1.1 μm and exhibit two-photon absorption at wavelengths below 2 μm, limiting their utility for pulsed and high-power applications in this range. This has led to CMOS-compatible dielectric waveguide systems such as silicon nitride [18], aluminium oxide [19] and tantalum pentoxide [20] being explored. Lasing in Er-doped [21] and Yb-doped [17] alumina and Nd-doped [22] and Er-doped [23] tantalum pentoxide have been demonstrated, and here we explore the suitability of tantalum pentoxide as a waveguide host for Yb ions.

Ta_2O_5 is a promising material for mass-producible, multifunctional, integrated photonic circuits on silicon, exhibiting excellent electrical, mechanical and thermal properties and good compatibility with complementary-metal–oxide–semiconductor (CMOS) technologies [24]. Its high refractive index ($n \approx 2.124$ at $\lambda \approx 980$ nm) [25], allows high index contrast between the waveguide core and silica cladding, providing for low-loss, tight bend radii thereby enabling the development of compact photonic circuits due to the strong confinement of the optical modes, and offering the potential for 2-D photonic crystal operation. Ta_2O_5 rib waveguide losses of ~0.2dB/cm have been obtained at a wavelength of 1.07 μm [22] and Ta_2O_5 is an excellent host for rare-earth ions, as demonstrated with neodymium [22] and erbium [23], and also provides a large third-order nonlinearity ($n_2 \approx 7.25 \times 10^{-19}$ m^2/W at $\lambda \approx 980$ nm) [20] for all-optical processing. In short, Ta_2O_5 offers high transparency and low two-photon absorption in the NIR compared with silicon, due to the bandgap being greater than 3.8 eV for Ta_2O_5, compared with 1.12 eV for silicon, corresponding to absorption band-edges at below $\lambda \approx 330$ nm for Ta_2O_5 compared with $\lambda \approx 1100$ nm for silicon, excellent rare-earth compatibility compared with silicon and silicon nitride, and high index-contrast and large third-order nonlinearity compared with aluminium oxide ($n \approx 1.726$; $n_2 \approx 0.31 \times 10^{-19}$ m^2/W at $\lambda \approx 1064$ nm [26]) rendering it of particular interest for the realization of mode-locked lasers.

In this paper, the design and fabrication of Yb:Ta_2O_5 rib waveguides using RF magnetron sputtering, photolithography and ion-beam milling is presented. The spectroscopic properties of Yb^{3+} ions in tantalum pentoxide (Ta_2O_5) such as the absorption and emission cross-sections, fluorescence spectrum and excited-state lifetime measurements are determined to allow the assessment of this material system to realize efficient high index contrast waveguide lasers.

2. Waveguide design and simulations

Channel waveguides in tantalum pentoxide were designed for single mode operation between 970 nm and 1100 nm, to cover the pump and signal wavelengths of an Yb-doped material. Waveguides were designed to be grown on oxidised silicon wafers and to have a silica cladding for symmetry and high index contrast. A partially etched rib waveguide approach, as shown in Fig. 1, was adopted to allow single mode operation of channels with widths readily fabricated using conventional photolithography, to maximise pump-signal overlap and to minimise waveguide loss due to sidewall roughness. The rib height was chosen to be 1μm to ensure good confinement of the modes within the core and the initial design was selected

#212073 - $15.00 USD Received 15 May 2014; revised 20 Jun 2014; accepted 20 Jun 2014; published 3 Jul 2014

using the approach of Soref et al. [27]. While an etch depth of up to 500 nm could be used and maintain monomode operation, an etch depth of 150 nm was chosen as a compromise between modal spotsize and loss due to sidewall roughness, leaving the outer slab thickness at 850 nm. With these constraints, waveguides with widths below 1.9 µm, readily achieved by conventional photolithography, were predicted to be monomode at a wavelength of 980 nm.

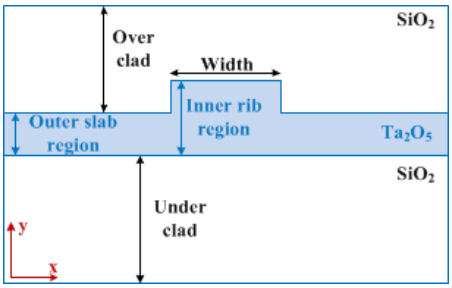

Fig. 1. Cross-section of the partially etched rib waveguide design.

The design was simulated and modal parameters extracted using finite element modeling (COMSOL) for a wavelength of 980 nm. Figure 2(a) shows the modal electric field profile for a rib width of 1 µm. Figure 2(b) shows the electric field in the horizontal (x-axis) and vertical (y-axis) directions across the point of peak intensity, extracted from Fig. 2(a). The full width at half maximum (FWHM) modal spotsize of a rib waveguide with a core height of 1 µm, width of 1 µm and etch depth of 150 nm in the y-axis is 0.6 µm and for the x-axis is 1.6 µm.

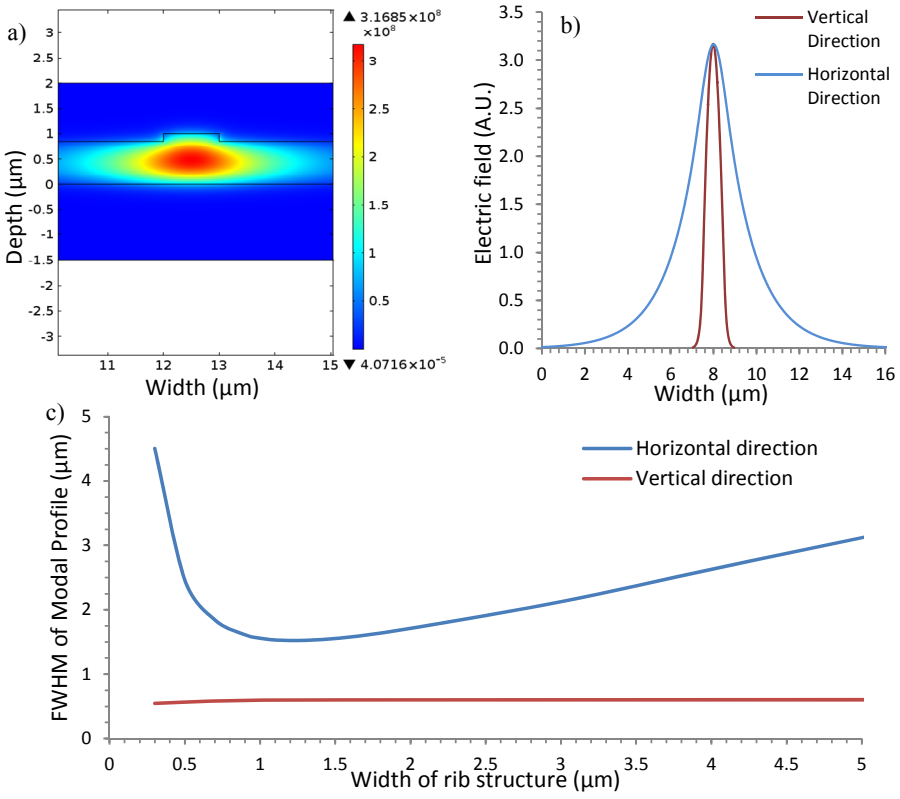

Fig. 2. COMSOL simulation of fundamental mode field for a rib waveguide with an etch depth of 150 nm: a) Normalised electric field for a rib width of 1 µm b) Electric field profiles in the horizontal and vertical directions; c) Modal spotsizes at FWHM intensity vs. rib width.

#212073 - $15.00 USD Received 15 May 2014; revised 20 Jun 2014; accepted 20 Jun 2014; published 3 Jul 2014

Figure 2(c) shows the modal spotsizes in the horizontal and vertical directions as a function of rib width, for the thicknesses defined above using the mode profiles calculated from COMSOL. It can be seen that for all waveguide widths the vertical spotsize remains flat at close to 0.6 μm while the horizontal spotsize is minimized at 1.52 μm for a rib width of 1.26 μm. Simulations showed that a design with the maximum 500 nm etch depth for monomode operation could yield a smaller and more nearly circular mode intensity profile with a spotsize of ≈0.6 μm for a 1 μm rib width. This may prove advantageous for the realization of a future Yb:Ta_2O_5 rib waveguide laser with low threshold.

3. Waveguide fabrication procedure

Nominally 1 μm thick Yb:Ta_2O_5 films were deposited by RF magnetron sputter deposition from a powder-pressed Ta_2O_5 target doped with 2.5 wt.% of ytterbium oxide (~$6.2x10^{20}$ Yb atoms/cm^3) onto a four inch silicon substrate with a 2.5 μm thick thermally-grown silica layer. The deposition was performed in a vacuum chamber which had been pumped to a base pressure of 10^{-8} Torr and then backfilled with a mixture of argon and oxygen. The conditions used for the deposition process were 20 and 5 sccm of argon and oxygen gas flow, respectively, substrate temperature of 200 °C and a magnetron power of 300 W; the chamber was maintained at a pressure of 10 mTorr. These conditions were previously optimized for Er:Ta_2O_5 to provide the lowest optical loss with an acceptable deposition rate [28].

Rib waveguides were realized, in accordance with the designs described above, using photolithography and argon ion beam milling (IBM). Strips of photoresist of widths varying from 1 to 10 μm in steps of 0.2 μm were defined in positive photoresist spun onto the deposited Yb:Ta_2O_5 film. The Yb:Ta_2O_5 film was then etched to a depth of 150 nm using an OIPT Ion Fab 300 Plus ion beam etch and deposition system. After etching and the removal of excess photoresist the wafer was treated in a bath of 30% aqueous potassium hydroxide (KOH) solution at a temperature of 55 °C for 20 minutes to reduce any surface roughness [28]. To reduce any stresses and oxygen deficiency introduced during the sputtering and etching processes the wafer was then annealed for two hours at 600 °C, with the furnace temperature ramped up at a rate of 3 °C per minute and ramped down at a rate of 2 °C per minute to room temperature [28].

A silica over-cladding of nominally 2 μm thickness was then deposited onto the patterned Yb:Ta_2O_5 waveguide core layer to produce symmetrical waveguides and to protect the core from external influences. The silica was sputtered using the same system as that used for the Yb:Ta_2O_5 layer. After the silica deposition, the wafer was again annealed at 600 °C to reduce oxygen deficiency and release the stresses introduced during the fabrication process. Prior to optical measurements the wafer was cut into smaller samples and end facets were polished to optical quality.

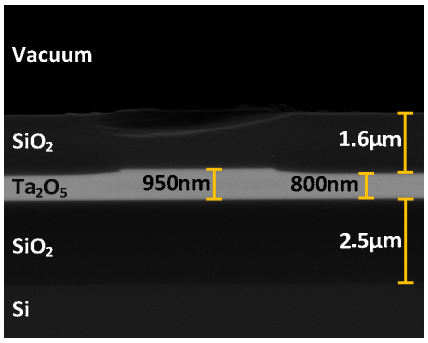

Fig. 3. SEM cross-section of a 3 μm wide rib waveguide showing the different optical layers. The lower layers are the silicon substrate with thermally-grown under-clad silica layer; the upper layers are the deposited Yb-doped Ta_2O_5 (light grey region) and silica over-clad.

#212073 - $15.00 USD Received 15 May 2014; revised 20 Jun 2014; accepted 20 Jun 2014; published 3 Jul 2014

An SEM cross-sectional image of the fabricated rib waveguide structure is shown in Fig. 3. The waveguide rib has a width of 3 μm and the thickness of the initial Yb:Ta_2O_5 film was found to be 0.95 μm, slightly smaller than the design value of 1 μm. The image shows that the rib side walls are not completely vertical and that a double slope structure is apparent. The sloped edges of the rib are expected to increase the modal spotsize in the horizontal direction, but will not significantly affect the spectroscopic measurements reported here. COMSOL modelling of a structure with sloped walls similar to those in Fig. 3 but otherwise with an identical design to that modelled in Fig. 2, shows that the sloped walls would increase the horizontal spotsize by 0.125 μm (8%) and affect the vertical spotsize by less than 0.5%.

The propagation loss of the waveguide was measured at a wavelength of 1064 nm, where ytterbium ion absorption is relatively weak. Light from a 1064nm laser diode was coupled into the waveguide using a monomode fibre and the waveguide output power was measured by collection with a multimode fibre, to arrive at an insertion loss. The input coupling loss was estimated by determining the increase in loss when the multimode output fiber was replaced by a single mode fibre identical to that used for input coupling. This coupling loss was then subtracted from the measured insertion loss to find the propagation loss, under the assumption that the input and output coupling loss to single mode fibre are identical and that the output coupling loss to multimode fiber is negligible. An upper limit on the propagation loss was found to be 3.9 dB/cm, but it is expected that there is a contribution to this from residual Yb absorption even at 1064nm.

The mode intensity profiles for undoped Ta_2O_5 waveguides at 980 nm were captured with a combination of a microscope objective lens and a CCD camera, and are shown in Fig. 4. For a rib waveguide of 5 μm width the experimental profiling gave a FWHM spotsize in the vertical and horizontal directions of 1.8 μm and 5.0 μm, respectively. The measured spotsizes are larger than predicted by the simulations in Fig. 2, which is to be expected due to the finite resolution of the imaging system, leading to an expected broadening of approximately 1.1 μm and, as described above, the non-verticality of the fabricated waveguide sidewalls which is expected to further increase the experimentally measured horizontal spotsize.

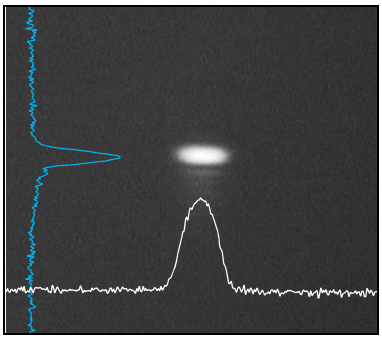

Fig. 4. Experimental mode profile for a 5 μm wide rib waveguide

4. Spectral characterization

In this section the measurement of the excited-state lifetime and the absorption and emission spectra of the Yb:Ta_2O_5 material, using the rib waveguides described above, and the resultant determination of the absorption and emission cross-sections are described. The excited-state lifetime and the absorption and emission cross-sections will enable the efficient design of a waveguide laser. These measurements have to be performed taking into account the effects of the waveguide configuration such as waveguide loss, the material/mode overlap factor and the potential for significant amplified spontaneous emission.

#212073 - $15.00 USD Received 15 May 2014; revised 20 Jun 2014; accepted 20 Jun 2014; published 3 Jul 2014

4.1 Absorption spectrum and cross-section

The unpolarized waveguide insertion loss spectrum was obtained using white light from a single-mode fiber-coupled broadband tungsten-halogen lamp. Light was coupled into a 3 mm long Yb:Ta_2O_5 rib directly from the single-mode fiber, and the light was coupled out of the waveguide end-facet into an optical spectrum analyzer (OSA) by means of a multimode fiber.

A reference measurement was made by measuring the output of the single-mode fiber directly to the input of the multimode fiber without the waveguide sample in place. The absorption spectrum includes loss contributions from fiber-waveguide coupling, propagation losses, and the Yb ion absorption. The absorption cross-section spectrum, $\sigma_{abs}(\lambda)$ was estimated from the insertion loss spectrum by subtracting the slowly-varying coupling and propagation loss baseline and using:

$$\sigma_{abs} = \ln(T) / NL \tag{1}$$

where T(λ) is the linear absorption, N is the density of Yb^{3+} ions and L is the waveguide length. Figure 5 shows the absorption cross-section where the length of the sample was taken to be 3 mm and the concentration of the ytterbium ions was estimated to be 6.2×10^{20} cm^{-3}.

It can be seen that the locations of the peak and sub-peak absorption are at 975 nm and 935 nm, corresponding to sub-levels in the $^2F_{7/2} \rightarrow {}^2F_{5/2}$ transition. While the insertion loss measurement is rather noisy, due to the low coupling efficiency from the standard monomode fiber to a waveguide with very small spotsize, it results in an acceptable estimate of the peak absorption cross-section at 975nm of $2.75 \pm 0.17 \times 10^{-20}$ cm^2.

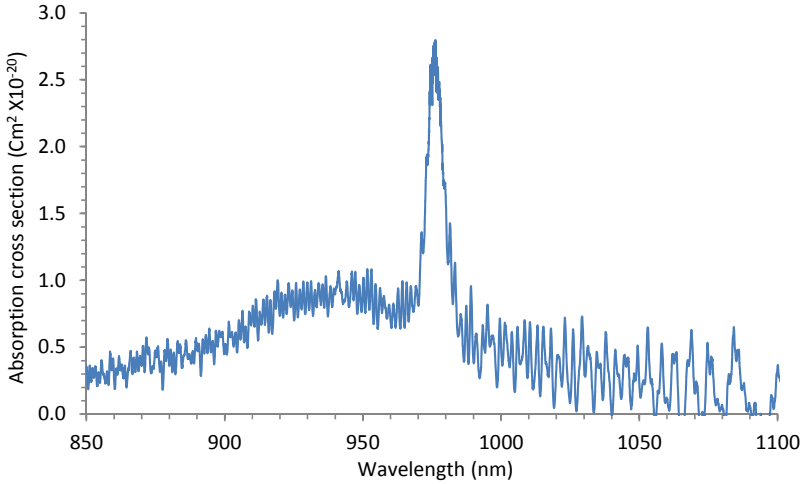

Fig. 5. Yb:Ta_2O_5 absorption cross-section.

4.2 Fluorescence spectrum and emission cross-section

For the measurement of the fluorescence of Yb:Ta_2O_5 the experimental setup used to acquire spectra consisted of a 971 nm fiber Bragg grating stabilized laser source butt-coupled via a single-mode fiber into an end-facet of a waveguide. The fluorescence was collected using a multimode fiber positioned above the waveguide close to the input, and fed directly into an OSA. The McCumber or reciprocity method [29,30] was used to estimate the emission cross-section from the absorption cross-section shown in Fig. 5. The accuracy of the deduced cross-section is poor at longer wavelengths due to the noise in the absorption spectrum and the nature of the McCumber transform, but is acceptable close to 977 nm, where the emission cross-section was estimated to be $\sigma_{em} = 2.90 \pm 0.73$ x10^{-20} cm^2. This was used as a scaling

#212073 - $15.00 USD Received 15 May 2014; revised 20 Jun 2014; accepted 20 Jun 2014; published 3 Jul 2014

factor to plot the emission cross-section spectrum from the fluorescence spectrum as shown in Fig. 6. The sharp peak at 971nm is due to scattered pump radiation.

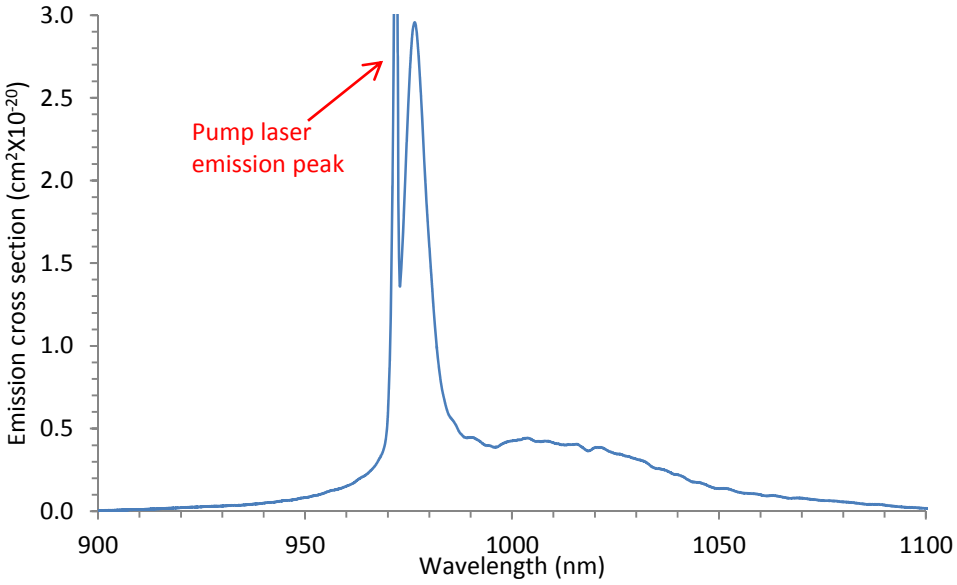

Fig. 6. Yb:Ta_2O_5 emission cross-section spectrum.

The emission cross-section spectrum, when pumped at a wavelength of 971 nm, comprises a broad emission band from 990 nm to 1090 nm with a separate strong peak at 977 nm similar to that reported in [1]. The broad emission bandwidth also shows similar magnitude to other Yb-doped glasses [31–33] which are a much larger than those seen with Yb-doped crystals [34–36].

4.3 Excited-state lifetime

The fluorescence lifetime measurement was performed on a 10.8 mm long Yb:Ta_2O_5 waveguide sample from the same wafer as that used for the absorption and fluorescence characterization. Light from the 971 nm pump laser diode was chopped at 200Hz using a mechanical chopper and focused into an end-facet of an Yb:Ta_2O_5 waveguide, with the pump power kept minimal to avoid significant amplified spontaneous emission (ASE). The light from the output of waveguide was propagated through a set of long pass filters with a cut-off wavelength of 1 μm to eliminate the pump wavelength. The resulting fluorescence power was then detected using a silicon photo-receiver connected to an oscilloscope. The time resolution of the system was approximately 20 μs. Figure 7 shows the fluorescent power vs. time, showing a lifetime of 260 ± 30 μs.

#212073 - $15.00 USD Received 15 May 2014; revised 20 Jun 2014; accepted 20 Jun 2014; published 3 Jul 2014

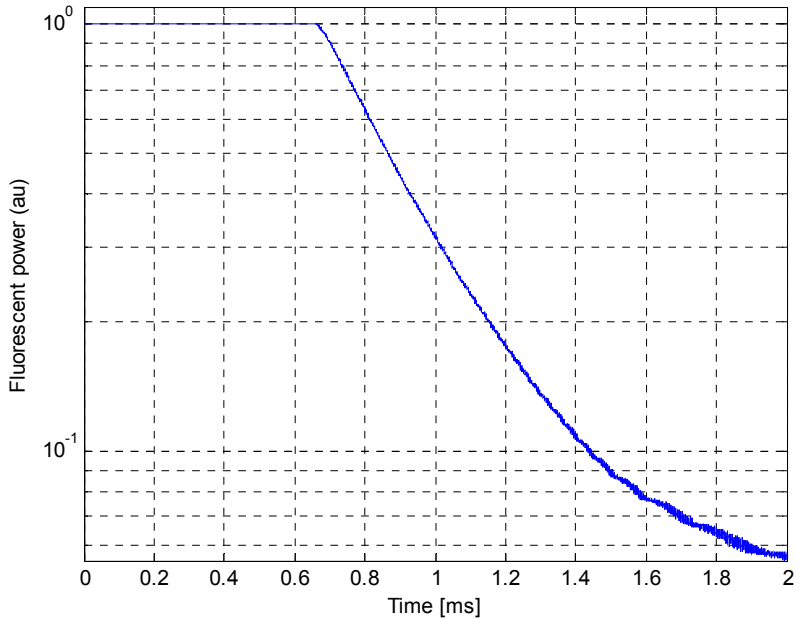

Fig. 7. Radiative decay curve.

5. Discussion

The absorption and emission cross-sections, fluorescence emission bandwidth and excited-state lifetime are key properties for Yb-doped lasing materials. Table 1 compares the spectroscopic properties of Yb:Ta_2O_5 determined here with published data for other Yb-doped materials.

Table 1. Comparison of the spectroscopic properties of the Yb:Ta_2O_5 studied in this work (red) with other Yb-doped glass (blue) and crystal (green) material systems

Host	Ta_2O_5	Bi_2O_3-based glass [1]	Silicate Q-246 [32]	Phosphate QX [32]	ZBLAN [33]	Tellurite 35PTY3Y [34]	$KY(WO_4)$ [35]
Ytterbium ion density, N, ($\times 10^{20} cm^{-3}$)	≈ 6.2	1.6	≈ 17	≈ 20	2 wt.% Yb	3.41	3
Pump Wavelength, λ_p, (nm)	971	975	970	970	911	974.9	981.2
Peak emission cross-section, σ_{em}, ($x10^{-20}$ cm^3)	2.9 @977nm	-	0.11 @970 nm	0.07 @970 nm	1.1* @975 nm	2.09 @975 nm	16* @980 nm
Peak absorption cross-section, σ_{abs}, ($\times 10^{-20}$ $cm^{3)}$	2.75 @975nm	2.1 @977 nm	0.19 @970 nm	0.25 @970 nm	1.1* @975 nm	1.55 @975 nm	13.3 @981.2 nm
Upper state life time, τ (ms)	0.26	0.55	1.1	1.3	1.7	0.96	0.6

*These cross-sections have been extracted from diagrams in the literature as accurately as possible

In comparison with other Yb-doped materials Yb:Ta_2O_5 has a broad emission bandwidth and large absorption and emission cross-section and has the added advantage of compatibility with CMOS processing.

As a figure of merit, the theoretical maximum gain of Yb:Ta_2O_5, with the dopant density used here, was calculated at the measured wavelength of peak emission using the measured

#212073 - $15.00 USD Received 15 May 2014; revised 20 Jun 2014; accepted 20 Jun 2014; published 3 Jul 2014

cross-section and assuming full inversion of Yb^{3+} ions, which may be approached when pumping at the short wavelength absorption sub-peak [9], using:

$$g_{mat} = 4.34 N_{inv} \sigma_{em} \quad (2)$$

Where g_{mat} is the material gain ($dBcm^{-1}$), σ_{em} is the peak emission cross-section, 2.9×10^{-20} cm^2 at 977 nm and N_{inv} is the inversion density. For full inversion, $N_{inv} = N = 6.2 \times 10^{20}$ cm^{-3}, yielding a maximum potential gain of 78 $dBcm^{-1}$. The combination of high potential gain with the broad bandwidth of Yb:Ta_2O_5 shows promise for modelocked laser applications.

Waveguide laser design and fabrication is ongoing, but the spectroscopic data reported in this paper allows the estimation of the launched pump power threshold for such a laser, using the approach of Fan [37]. In the case of 5mm long waveguide with a 99% reflectivity input coupler, a 95% output coupler and a propagation loss of 4 dB/cm, the predicted launched pump power threshold was estimated to be ~10 mW. The waveguide losses reported here are believed to be an overestimate due to residual Yb absorption at the measurement wavelength of 1064nm and lower waveguide losses such as those reported in [22] would reduce this threshold significantly.

6. Conclusion

The spectroscopic properties of Yb:Ta_2O_5 as a new waveguide laser material have been studied, and the absorption and emission cross-sections and excited-state lifetime determined. Rib waveguides operating in a single mode between 970 nm and 1100 nm for widths less than 1.9 μm were realized on silicon substrates using CMOS fabrication technologies. The peak absorption cross-section was measured to be 2.75×10^{-20} cm^2 at 975 nm. The emission spectrum was found to be typical of Yb-doped materials in the wavelength region around 1 μm, with a broad fluorescence spanning from 990nm to 1090 nm, the fluorescence peak occurring at a wavelength of 976 nm, with a peak emission cross-section of 2.9×10^{-20} cm^2. The upper state life time was measured to be 260 ± 30 μs. This material system shows promise for advanced compact lasers with monolithically integrated components to add functionality, such as ring resonators exploiting the high index contrast and nonlinear components for switching or modelocking, exploiting the high third order nonlinearity of tantalum pentoxide [20]. Furthermore, the broad emission bandwidth makes the material appropriate for mode-locking and ultra-short pulse generation and progress towards an ytterbium-doped waveguide laser in Ta_2O_5 is underway.

Acknowledgment

This work was partly supported by the UK EPSRC through Platform Grant EP/J008052/1 “Integrated Photonic Materials and Devices”.